Computers and Structures 88 (2010) 806–811

Contents lists available at ScienceDirect

Computers and Structures

journal homepage: www.elsevier.com/locate/compstruc

Technical Note

Multiobjective topology optimization for finite periodic structures

Yuhang Chen, Shiwei Zhou, Qing Li *

School of Aerospace, Mechanical and Mechatronic Engineering, The University of Sydney, Sydney, NSW 2006, Australia

ARTICLE INFO

Article history:
Received 2 September 2009
Accepted 16 October 2009
Available online 20 November 2009

Keywords:
Topology optimization
Multiobjective
Periodic structure
Sensitivity analysis
Multicomponents
Pareto optimum

ABSTRACT

Many engineering structures consist of specially-fabricated identical components, thus their topology optimizations with multiobjectives are of particular importance. This paper presents a unified optimization algorithm for multifunctional 3D finite periodic structures, in which the topological sensitivities at the corresponding locations of different components are regulated to maintain the structural periodicity. To simultaneously address the stiffness and conductivity criteria, a weighted average method is employed to derive Pareto front. The examples show that the optimal objective functions could be compromised when the total number of periodic components increases. The influence of thermoelastic coupling on optimal topologies and objectives is also investigated.

1. Introduction

Engineering structures are often devised with two significant features. Firstly, most structures are expected to function in different physical conditions; and secondly, many structures comprise some identical components or parts for mass production, storage and transportation benefits. This is why the structural optimization of outstanding multifunctional objectives with periodic components is of particular importance in engineering context.

Over the last two decades, topology optimization has been developed as an effective tool to seek the optimal configuration of a structure for multidisciplinary criteria in a specified design domain [1–5], in which substantial efforts have been devoted to different algorithms, formulations and solutions to various individual criteria, ranging from mechanical [1,2,4–6] to thermal [7–9], permeable [10,11] and magnetic [12] objectives. Some attempts have been made to optimize various coupled multiphysical systems, e.g. piezoelectric [13,14], thermoelastic [15–19] and thermoelectrical [20,21] designs.

One of the main challenges confronted in topology optimization is the involvement of more than one design objective, in particular, those competing criteria [22,23]. It is often difficult to achieve all the design objectives simultaneously and certain trade-off must be made during the design. To cope with this issue, an accepted alternative is to derive a Pareto optimum, where a Pareto front is generated and the multiple objectives are optimized in a compromise manner. In this respect, the linear weighting function scheme (i.e. arithmetic average) has been extensively applied to search for multiobjective optimum provided that the Pareto front is convex. It is noted that the thermoelastic problems have been often exemplified to demonstrate such design features. Li et al. [24] and Kim et al. [25] adopted the weighting factor method to combine thermal stress and heat flux for a unified design criterion, and showed that varying the weights led to different topologies. de Kruijf et al. [26] incorporated the stiffness and conduction criteria into a single cost objective for 2D structural and material designs. However, a more thorough study is still needed, particularly to explore the relationship between multiobjective optimal topologies and corresponding Pareto fronts.

Another key issue that remains to be under-investigated is the topology optimization for periodic structures that comprise a finite number of identical components or parts. Unlike the periodic materials whose base cells are generally many orders smaller than the materials sample considered [27,28], the sizes of periodic components are often comparable to the entire structural system. In this scenario, external boundary and loading conditions could significantly affect each component to different extents, making their performances inhomogeneous [29]. Thus the typical homogenization technique [30] may not be applicable for relating the global properties to base cell (component) characteristics. In other words, the inverse homogenization algorithms [27] developed for periodic material design may be inapplicable. To tackle this problem, Zhang and Sun [31] developed a two-level design approach by combining the macroscopic optimization with microscopic optimization. More recently, Huang and Xie [32] established a mono-scale approach to the optimization of periodic structures, by simply averaging the sensitivities at corresponding locations of each component to maintain the structural periodicity. In these two articles, however, only a simple stiffness criterion has been considered.

* Corresponding author. Tel.: +61 2 9351 8607; fax: +61 2 9351 7060.
E-mail address: q.li@usyd.edu.au (Q. Li).

0045-7949/$ - see front matter © 2009 Elsevier Ltd. All rights reserved.
doi:10.1016/j.compstruc.2009.10.003

This paper aims to develop a unified procedure for 3D multiobjective topology optimization of finite periodic structures. Without loss of generality, the minimizations of mechanical and thermal compliances are adopted as the design objectives herein. A number of examples are presented to explore the topologies, Pareto fronts and assembly patterns.

2. Statement of the problem and sensitivity analysis

The finite element solutions to elastic and thermal governing equations determine the displacement field $\mathbf{u}$ and temperature field ϕ, which allow us to assess the mechanical and thermal performances of a specific structure in terms of the compliances. It is deemed that the lower the mechanical and thermal compliances, the better the corresponding performances. In a multiobjective framework, the design problem can be accordingly formulated in terms of weighting factors w_s and w_c, as

$$\begin{cases} \min F = w_s f_s + w_c f_c \\ \quad = \sum_{e=1}^{NE} \left[w_s \dfrac{(\mathbf{u}_s^e + \tau \mathbf{u}_c^e)^T (\rho^e)^{p_s} \mathbf{K}_s^e (\mathbf{u}_s^e + \tau \mathbf{u}_c^e)}{C_s^*} + w_c \dfrac{(\boldsymbol{\phi}^e)^T (\rho^e)^{p_c} \mathbf{K}_c^e (\boldsymbol{\phi}^e)}{C_c^*} \right] \\ \text{s.t.} \quad \sum_{e=1}^{NE} V^e \rho^e = V_t; \quad 0 \leqslant \rho_{\min} \leqslant \rho^e \leqslant 1, \quad \tau = 0, 1; \\ \quad e = 1, 2, \ldots, NE \end{cases} \tag{1}$$

where f_s and f_c are mechanical and thermal compliance objectives, respectively. NE denotes the total number of elements, V_t the volume constraint and ρ_{min} represents the lower limit of design variable ρ^e (relative density), preventing finite element analysis from singularity [33–35]. u_s^e, u_c^e and ϕ^e are the elemental displacement vectors due to the mechanical and thermal loadings and elemental temperature vector, respectively. K_s^e and K_c^e are the elemental stiffness and conductivity matrices. C_s^* and C_c^* are the maximum structural and thermal compliances which are used to normalize these two different objective functions to a range of 0–1. p_s and p_c are two parameters used in the SIMP model to penalize intermediate densities towards a 0–1 design [1]. w_s and w_c, which are chosen such that the sum equals unity, i.e. $w_s + w_c = 1$, represent two weighting factors to control the proportion or emphasis between mechanical and thermal objectives.

The sensitivity of ith element for the bi-objective optimization problem defined in Eq. (1) can be given as,

$$\frac{\partial F}{\partial \rho^i} = -w_s p_s \frac{(\mathbf{u}_s^i + \tau \mathbf{u}_c^i)^T (\rho^i)^{(p_s-1)} \mathbf{K}_s^i (\mathbf{u}_s^i + \tau \mathbf{u}_c^i)}{C_s^*} - w_c p_c \frac{(\boldsymbol{\phi}^i)^T (\rho^i)^{(p_c-1)} \mathbf{K}_c^i (\boldsymbol{\phi}^i)}{C_c^*} \tag{2}$$

It should be noted that in the finite periodic structure, the difference of two physical fields in different components make the sensitivities non-periodic, thereby leading to a non-periodicity of different components after optimization. To avoid such a paradox, Huang and Xie [32] proposed a simple yet effective method, in which all the sensitivities at the corresponding locations of different components are averaged as

$$\frac{\partial F}{\partial \rho^{i,j}} = -\frac{1}{NP} \sum_{j=1}^{NP} \left[\begin{array}{l} w_s p_s \dfrac{\left(\mathbf{u}_s^{i,j} + \tau \mathbf{u}_c^{i,j}\right)^T (\rho^{i,j})^{(p_s-1)} \mathbf{K}_s^{i,j} \left(\mathbf{u}_s^{i,j} + \tau \mathbf{u}_c^{i,j}\right)}{C_s^*} \\ + w_c p_c \dfrac{(\boldsymbol{\phi}^{i,j})^T (\rho^{i,j})^{(p_c-1)} \mathbf{K}_c^{i,j} (\boldsymbol{\phi}^{i,j})}{C_c^*} \end{array} \right] \tag{3}$$

where $(\cdot)^{i,j}$ denotes the ith element in the jth component and $NP = n_x \times n_y \times n_z$ is the total number of components. By doing so, a unified sensitivity of different components is provided, which allows us to optimize the topologies of different components in a consistent way. Consequently, the structural periodicity can be retained via such a variable-linking technique as indicated in Eq. (3), in which the elemental densities at corresponding locations are preserved to have the same value, thereby maintaining the periodicity during the design.

3. Results and discussion

In this section, we will present three demonstrative examples to illustrate the bi-objective designs with or without coupling effect for both conventional ($1 \times 1 \times 1$) and finite periodic topology optimizations. All the 3D design domains are discretized into unit cubic elements and the initial density fields are of uniform material distribution where volume fraction is equal to the prescribed one. In this paper, the penalty factors used in the SIMP models for the Young's modulus and conductivity are both set as $p_s = p_c = 3$ [36]. During the optimization process, it will not be considered convergent until the maximum density change in any element is less than 0.1% in 10 consecutive iterations.

3.1. Conventional structural designs with bi-objectives

As shown in Fig. 1(a), the design domain is evenly heated at all nodes in this example. At the center on the bottom surface, there is a heat sink, whose temperature is kept to be zero degree. Four corners of the bottom surface are kinematically fixed and a unit force is applied along the x-axis at the center of the upper surface. Due to the double-symmetry of the structure, we only analyze a quarter of the design domain that is discretized into $80 \times 40 \times 40$ unit cubic elements. The Young's modulus, Poisson's ratio and the conductivity of solid materials are set to 1, 0.3 and 1, and the constraint of volume fraction is 30%, respectively.

By varying w_s from 1 (the full stiffness design) to 0 (the full conduction design), the optimal structural topologies are generated as shown in Fig. 1. It is interesting to see how the mechanical and thermal objectives compete with each other and make significant influence on the topological designs. In the full stiffness design ($w_s = 1$, Fig. 1(a)), the four bars connect the fixed corner boundary with the loading point to best support the external mechanical force. On the other hand, in the full conduction design ($w_s = 0$, Fig. 1(b)), the material is mostly distributed near the heat sink and spread out along a doubly-symmetric tree-like configuration with numerous fine twigs. In this case, there is no any connection between the kinematic boundary (the four bottom corners) and the mechanical loading point. However, if slightly increase the stiffness weight (e.g. $w_s = 0.001$), an evident connection near the load point can be observed as shown in Fig. 2(a). Further increase in the stiffness weight will strengthen the connection of loading point to kinematic boundary and weaken the heat dissipation from the heat

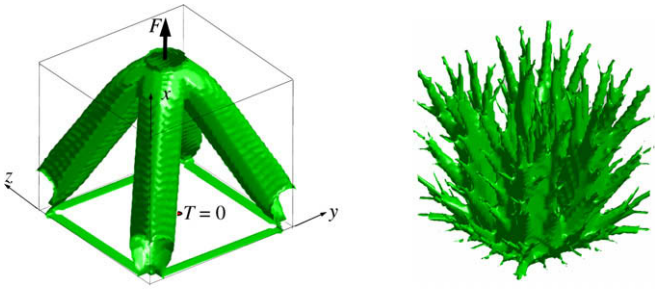

(a) $w_s = 1.000$ (b) $w_s = 0.000$

Fig. 1. Two extreme cases in conventional bi-objective structural designs.

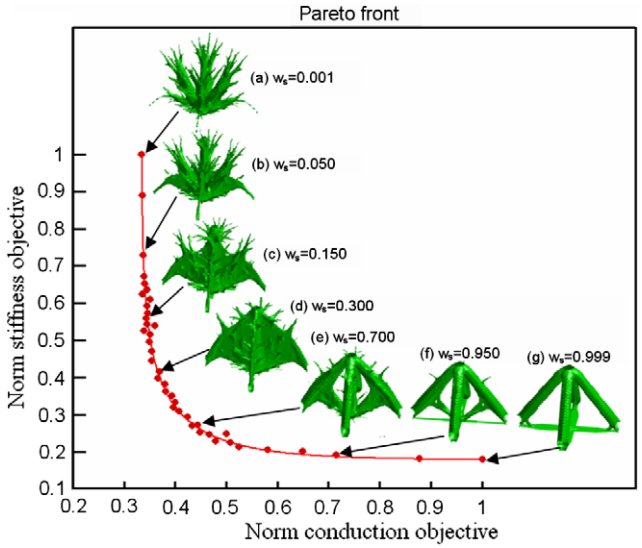

Fig. 2. Pareto front and corresponding structural topologies.

sink (Fig. 2(b)–(f)). It is worth noting that there is a sudden change in the material distribution on the bottom surface between Fig. 1(a) and Fig. 2(g). A cross-bar connecting the four fixed corners and heat sink is presented due to presence of only 0.1% conduction objective (Fig. 2(g)), while the four thin bars connecting the fixed corners emerge in the full stiffness design to keep the whole structure stiffest (Fig. 1(a)).

Fig. 2 plots the Pareto front which shows how those two objectives compete with each other and how the topologies vary along with the change in the objective weights. In this example, a clear convexity of the Pareto curve can be observed. It should be noted that these two extreme cases, i.e. the full stiffness and conductivity designs, are not included in Pareto front, since the singularity makes the objectives too far away from the illustratable area to be shown. In this curve, it is observed that any further reduction in one objective must sacrifice another objective. For example, in the region near the full conduction design (i.e. the upper-left part of the Pareto front) the mechanical compliance drops rapidly, while the thermal compliance only slightly increases, and *vice versa*. This 3D version of topology optimization exhibits a similar trend to the 2D counterparts [26].

3.2. Finite periodic structural designs without thermoelastic coupling ($\tau = 0$)

Consider a vertical cantilever structure as shown in Fig. 3(a) with a heat sink at the center of its bottom surface and four transverse loads applied at the upper corners. The design domain is divided into $72 \times 36 \times 36$ unit cubic elements. A volume fraction constraint of 10% is prescribed in this example. All the other parametric settings, including material properties, remain the same as those in the previous example.

In this example, several different assembly patterns of components are considered. The full stiffness ($w_s = 1; w_c = 0$) and full conductivity ($w_s = 0; w_c = 1$) designs are presented first, followed by the various bi-objective designs. Finally, several different Pareto fronts are plotted to explore the competitive relations between these two design criteria.

3.2.1. Periodic structural designs for full stiffness and full conductivity

Fig. 3 shows the optimized topologies for different assembly patterns with the typical full stiffness designs. For the $1 \times 1 \times 1$ single-component structure (i.e. a conventional topology optimization), it is seen that the final topology takes a shape in the two sidely-positioned plates, each connecting the loading points on the top face to the fixed kinematic boundary points on the base. Surprisingly, the $2 \times 1 \times 1$ (denoting 2 components in x, 1 in y and 1 in z-directions) periodic structure, shown in Fig. 3(b), has a similar topology to the $1 \times 1 \times 1$ design. It is worth noting that the height of rectangular $1 \times 1 \times 1$ structure is twice of the width, resulting in two similar crossed frames, one on the top of the other, to maximize the stiffness in the design of $1 \times 1 \times 1$ configuration, while the components in $2 \times 1 \times 1$ periodic structure have a shorter height, where each of them forms only a single crossed frame. Interestingly, the similar topological resemblance can be seen again between Fig. 3(d) and (f). It appears that the aspect ratio of components (height vs. width) largely determines the final optimal topology in the finite periodic structural design.

On the other hand, Fig. 4 illustrates other four different periodic structures for the full conductivity designs. In the conventional single component design ($1 \times 1 \times 1$), a similar topology to Fig. 1(b) can be observed. Regarding the $2 \times 1 \times 1$ structure, the periodicity treatment of sensitivity results in a pseudo heat sink, which emerges at the center of design domain to form another tree-like topology in the upper part. Compared Fig. 4(c) with Fig. 4(d), i.e. $2 \times 2 \times 1$ with $2 \times 3 \times 1$ periodic structures, it is seen that the number of periodicity in y-axis somewhat influences the final topologies. When an even periodicity in y-axis is presented, e.g. Fig. 4(c), the pseudo heat sinks emerge in the lateral sides, producing halves of tree-like structures. On contrary, when an odd periodicity in y-axis is presented, e.g. Fig. 4(d), the pseudo heat sinks emerge inside, showing integrated periodicities.

Tables 1 and 2 compare the mechanical and thermal compliances in different periodic structures for the full stiffness and full conduction designs, respectively. It is interesting to note that both of them demonstrate a certain increase in the resulted mechanical or thermal compliances as the increase in the periodicity manifolds. This tendency obtained in the mechanical case is in a good agreement with those in literatures [31,32].

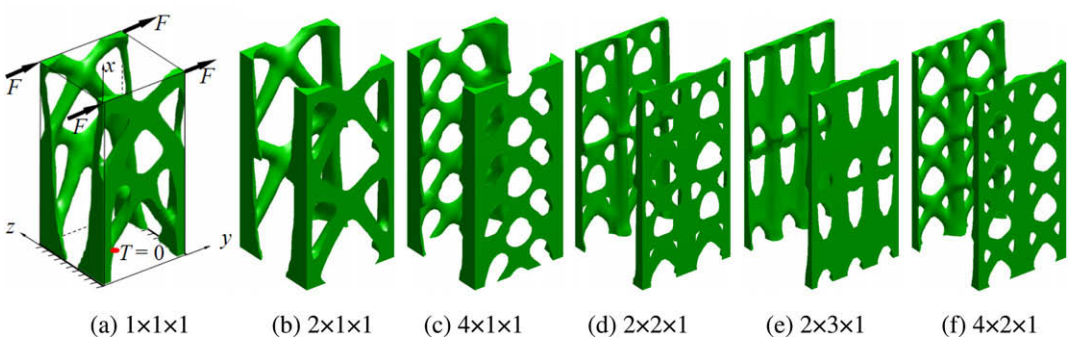

Fig. 3. Full stiffness designs for periodic structures without thermoelastic coupling.

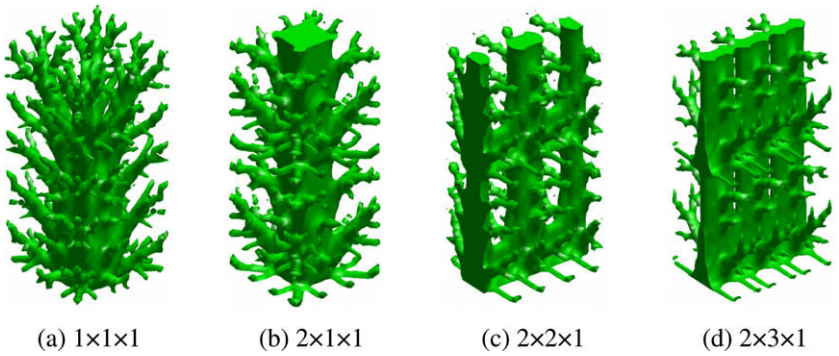

Fig. 4. Full conductivity designs for periodic structures without thermoelastic coupling.

Table 1
Mechanical compliances of different periodic structures for the full stiffness designs.

	$1 \times 1 \times 1$	$2 \times 1 \times 1$	$4 \times 1 \times 1$	$2 \times 2 \times 1$	$2 \times 3 \times 1$	$4 \times 2 \times 1$
Mechanical compliance	66.36	68.45	71.69	72.12	72.67	74.98

Table 2
Thermal compliances of different periodic structures for the full conductivity designs.

	$1 \times 1 \times 1$	$2 \times 1 \times 1$	$2 \times 2 \times 1$	$2 \times 3 \times 1$
Thermal compliance	1014.4	1047.2	1115.3	1181.5

3.2.2. Bi-objective designs and Pareto fronts

In this section, we will further look at the bi-objective designs for periodic structures. For the sake of simplicity, the conventional structure ($1 \times 1 \times 1$) is firstly exemplified to observe topological variation, followed by the discussion of the relationship between the number of components and the corresponding Pareto's fronts.

By employing the same methodology used in the previous example, a series of optimized topologies can be obtained by varying the stiffness weight w_s, as summarized in Fig. 5. Starting from the familiar tree-like topology (Fig. 5(a)), a significant variation in topology takes place when only 1% of stiffness objective is taken into account as in Fig. 5(b). It can be seen that the two crossed-bars are taking shape in the region near the upper loading area and assembled against the kinematical boundary in the bottom to form a 'V'-shaped configuration in the front view (in y-direction). The domain close to the heat sink is again dominated by the tree-like configuration to promote heat dissipation but the fine twigs have been greatly suppressed. As w_s continues to increase, the connective material between two opposite parts is gradually weakened, finally forming two separate Michell-type sub-structures (Fig. 5(c)–(e)).

Fig. 6 plots the Pareto fronts for three different periodic structures. Similarly to Fig. 2, all the Pareto curves are convex, indicating an effectiveness of employing the linearly weighted factor method in such a bi-objective optimization. Comparing these three Pareto curves, it is clearly observed that the Pareto curve of $3 \times 3 \times 1$ is overall higher than that of $3 \times 1 \times 1$; and the one of $3 \times 1 \times 1$ is overall higher than that of $1 \times 1 \times 1$, consistently. This clearly indicates that the more the components there are, the worse the Pareto optimum. It is considered logical because the sensitivities are averaged among different components in order to maintain the structural periodicity, the larger the number of components, the more the sacrifices in the sensitivity. Furthermore, after the sensitivity averaging technique has been applied, some implicit (pseudo) constraints which can be observed in Figs. 3 and 4 come out, making the achieved optima worse. Thus, such sensitivity averaging technique indeed worsens the optimization as the number of components increases.

It should be noted here that, a major variation in topology only happens when w_s varies in a small region of $0 \leqslant w_s \leqslant 0.25$ and a majority of solution points and corresponding topologies are not evenly distributed near the Pareto curves. In other words, the mechanical criterion seems to have a greater influence in the final structural topologies than the thermal criterion in this example. For the thermal criterion, disperse twigs are required to better dissipate the thermal energy. Unfortunately, such topological features

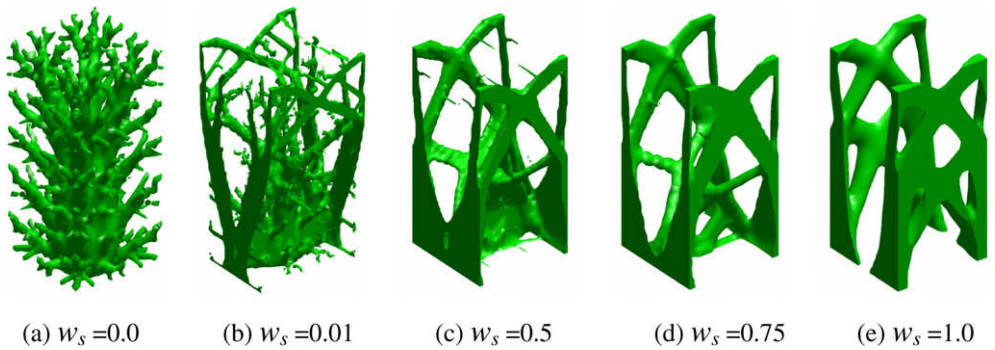

Fig. 5. Periodic structural designs with increscent stiffness weighting factors (without thermoelasticity).

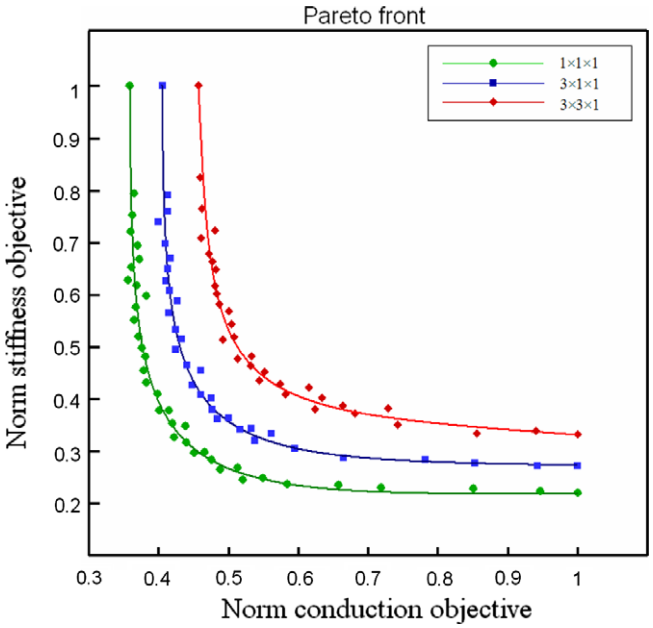

Fig. 6. Pareto fronts of different periodic structures (without thermoelasticity).

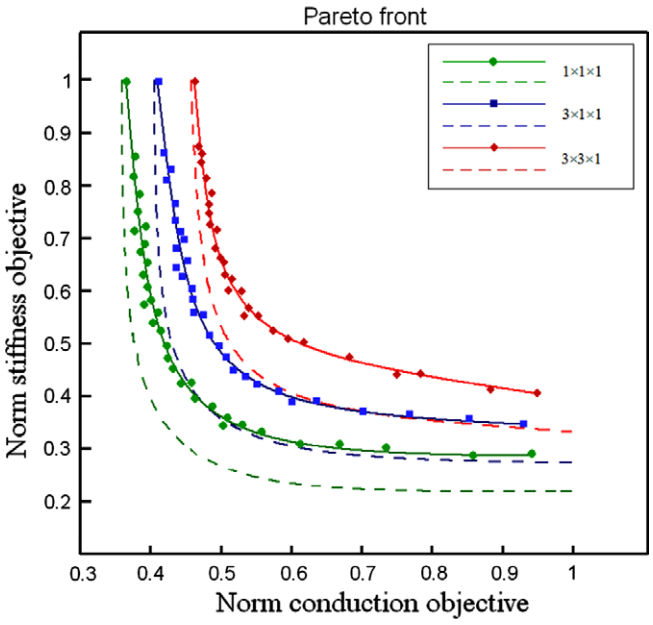

Fig. 8. Pareto fronts for finite periodic structures with thermoelastic coupling. Dashed curves indicate the Pareto fronts without thermoelasticity.

make little contribution to the mechanical stiffness. For the stiffness criterion design, on the other hand, majority of solid structures is concentrated to transfer the mechanical loads to kinematical boundary in a stiffest way. But this allows keeping certain capacities to transmit thermal energy. For this reason, the thermal criterion could be sacrificed severely even when w_s takes a small value in order to minimize these two competing objectives concurrently.

3.3. Finite periodic structural designs with thermoelastic coupling ($\tau = 1$)

In this section, the designs for finite periodic structures with thermoelastic coupling will be carried out. In order to identify thermoelastic influence in the final optimal topologies, the similar design problem that was used in the previous example is employed herein again. In this example, the Young's modulus E is set to 210 GPa, Poisson's ratio $\nu = 0.3$, thermal conductivity $\kappa = 50\ \mathrm{W\ m^{-1}\ K^{-1}}$ and thermal expansion coefficient $\alpha = 1.2 \times 10^{-5}\ \mathrm{K^{-1}}$.

From the mechanical point of view, the stress field induced by pure bending is distributed oppositely against the neutral axis. However, a symmetrical thermal displacement field is obtained owing to the double-symmetry in the thermal conductivity problem. After the superposition of the mechanical and thermal displacement fields, the final coupling shows a non-symmetrical distribution, hereby producing a non-symmetrical sensitivity field and causing structural difference in the final topologies.

Fig. 7 exhibits the influence of thermoelastic coupling on the multiobjective optimization. Controlled by weighting factor w_s, there is no thermoelastic effect in the full conduction design. As w_s increases, the stiffness objective becomes more and more dominant and thus the non-symmetry of material distribution becomes stronger in the region near the heat sink. It is logical that the materials tend to distribute more in the tensile portion of cantilever beam, since the total tensile displacements are amplified after considering the thermal expansion. However, when w_s exceeds 0.98, the thermoelasticity enforces majority of the material to distribute in the lower part of design domain, making loading points disconnect from the kinematic boundaries and causing the FEA to become singular.

Fig. 8 plots the Pareto fronts, which show how the thermoelastic coupling influences the multiobjective optimization. Interestingly, after considering coupled thermoelastic effect, the mechanical compliance is significantly increased (worsened stiffness), while the thermal compliance remains unchanged at all these three cases.

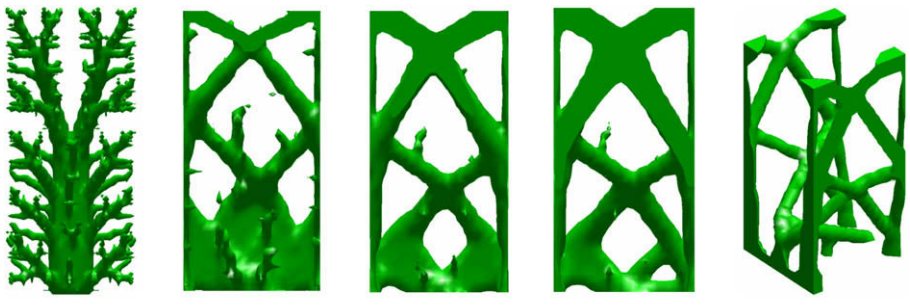

(a) w_s =0.0 (b) w_s =0.05 (c) w_s =0.5 (d) w_s =0.8 (e) w_s =0.98

Fig. 7. Periodic structural designs with increasing stiffness weight (thermoelastic coupling).

4. Concluding remarks

This paper presented a unified procedure for 3D multiobjective finite periodic structural optimization. In finite periodic structures, the characteristic length is comparable with the dimension of components. Thus the influence of non-periodic boundary conditions in these components must be taken into account and the homogenization method that was derived for infinite periodic materials may become inapplicable. A simple sensitivity averaging technique was adopted to avoid the inconsistency induced by non-periodic boundaries, hereby optimizing the topologies of all the components simultaneously and preserving the structural periodicity in the design process. In this study, a multiphysical problem of minimizing the mechanical and thermal compliances was formulated in terms of linear weighting factors, which allowed optimizing the structure for these competing criteria.

The proposed methodology was demonstrated through the designs of 3D finite periodic structures toward the maximum stiffness and thermal conduction. By varying the weighting factors for different criteria, a series of optimal solutions were generated, forming the Pareto front in design space. All the illustrative examples clearly showed the significant variations in the optimal topologies and a strongly competing relationship between those two criteria, in either conventional or finite periodic designs, with or without thermoelastic coupling. Although the linear weighting method was used in this study to deal with multiobjective optimization problems, it should be noted that other more sophisticated methods, such as Normal Boundary Intersection (NBI) [37] and Physical Programming (PP) [38], could be adopted to possibly yield a more uniform point distribution along the Pareto front.

It is also concluded that, firstly, the optimal mechanical and thermal compliances become higher when the total number of components increases, which implies that the conventional structural design provides the best performance under the same loading and boundary conditions but may sacrifice manufacturability when the structural dimension is prohibitively large. Secondly, the inclusion of thermoelastic properties leads to a certain reduction in the global mechanical stiffness but maintains almost the same level in the conduction. Thirdly, the mechanical criterion has a greater influence in the optimal topologies than the thermal criterion in the given examples.

Acknowledgements

The support from Australian Research Council (ARC) is greatly acknowledged. The first author is grateful for the Faculty Scholarship at The University of Sydney. The authors also acknowledge the anonymous reviewers for their valuable comments.

References

[1] Bendsøe MP. Optimal shape design as a material distribution problem. Struct Optim 1989;1:193–202.
[2] Bendsøe MP, Kikuchi N. Generating optimal topologies in optimal design using a homogenization method. Comput Methods Appl Mech Eng 1988;71:197–224.
[3] Allaire G, Jouve F, Toader AM. Structural optimization using sensitivity analysis and a level-set method. J Comput Phys 2004;194:363–93.
[4] Xie YM, Steven GP. A simple evolutionary procedure for structural optimization. Comput Struct 1993;49:885–96.
[5] Hinton E, Sienz J. Fully stressed topological design of structures using an evolutionary procedure. Eng Comput 1995;12:229–44.
[6] Li Q, Steven GP, Xie YM. Evolutionary structural optimization for stress minimization problems by discrete thickness design. Comput Struct 2000;78:769–80.
[7] Li Q, Steven GP, Xie YM, Querin OM. Evolutionary topology optimization for temperature reduction of heat conducting fields. Int J Heat Mass Transf 2004;47:5071–83.
[8] Zhou SW, Li Q. The relation of constant mean curvature surfaces to multiphase composites with extremal thermal conductivity. J Phys D-Appl Phys 2007;40:6083–93.
[9] Bruns TE. Topology optimization of convection-dominated, steady-state heat transfer problems. Int J Heat Mass Transf 2007;50:2859–73.
[10] Guest J, Prévost JH. Design of maximum permeability material structures. Comput Methods Appl Mech Eng 2006;196:1006–17.
[11] Guest J, Prévost JH. Optimizing multifunctional materials: Design of microstructures for maximized stiffness and fluid permeability. Int J Solids Struct 2006;43:7028–47.
[12] Yoo J, Hong H. A modified density approach for topology optimization in magnetic fields. Int J Solids Struct 2004;41:2461–77.
[13] Silva ECN, Fonseca JSO, Kikuchi N. Optimal design of piezoelectric microstructures. Comput Mech 1997;19:397–410.
[14] Rohan E, Miara B. Homogenization and shape sensitivity of microstructures for design of piezoelectric bio-materials. Mech Adv Mater Struct 2006;13:473–85.
[15] Rodrigues H, Fernandes P. A material based model for topology optimization of thermoelastic structures. Int J Numer Methods Eng 1995;38:1951–65.
[16] Li Q, Steven GP, Xie YM. Displacement minimization of thermoelastic structures by evolutionary thickness design. Comput Methods Appl Mech Eng 1999;179:361–78.
[17] Xia Q, Wang MY. Topology optimization of thermoelastic structures using level set method. Comput Mech 2008;42:837–57.
[18] Bruns TE. Topology optimization by penalty (TOP) method. Comput Methods Appl Mech Eng 2007;196:4430–43.
[19] Li Q, Steven GP, Xie YM. Thermoelastic topology optimization for problems with varying temperature fields. J Thermal Stress 2001;24:347–66.
[20] Torquato S, Hyun S, Donev A. Multifunctional composites: optimizing microstructures for simultaneous transport of heat and electricity. Phys Rev Lett 2002;89:266601-1–1-4.
[21] Torquato S, Hyun S, Donev A. Optimal design of manufacturable three-dimensional composites with multifunctional characteristics. J Appl Phys 2003;94:5748–55.
[22] Anskanen P. A multiobjective and fixed elements based modification of the evolutionary structural optimization method. Comput Methods Appl Mech Eng 2006;196:76–90.
[23] Steven GP, Li Q, Xie YM. Multicriteria optimization that minimizes maximum stress and maximizes stiffness. Comput Struct 2002;80:2433–48.
[24] Li Q, Steven GP, Querin OM, Xie YM. Structural topology design with multiple thermal criteria. Eng Comput 2000;17:715–34.
[25] Kim MS, Kim R, Han SY, Yi BJ. Topology optimization of a PCB substrate considering mechanical constraints and heat conductivity. J Mech Sci Technol 2007;21:2041–7.
[26] de Kruijf N, Zhou SW, Li Q, Mai YM. Topological design of structures and composite materials with multiobjectives. Int J Solids Struct 2007;44:7092–109.
[27] Sigmund O. Materials with prescribed constitutive parameters – an inverse homogenization problem. Int J Solids Struct 1994;31:2313–29.
[28] Sigmund O. Tailoring materials with prescribed elastic properties. Mech Mater 1995;20:351–68.
[29] Tantikom K, Aizawa T, Mukai T. Symmetric and asymmetric deformation transition in the regularly cell-structured materials. Part I: Experimental study. Int J Solids Struct 2005;42:2199–210.
[30] Hassani B, Hinton E. A review of homogenization and topology optimization I—homogenization theory for media with periodic structure. Comput Struct 1998;69:707–17.
[31] Zhang WH, Sun SP. Scale-related topology optimization of cellular materials and structures. Int J Numer Methods Eng 2006;68:993–1011.
[32] Huang X, Xie YM. Optimal design of periodic structures using evolutionary topology optimization. Struct Multidiscip Optim 2008;36:597–606.
[33] Sigmund O. A 99 line topology optimization code written in Matlab. Struct Multidiscip Optim 2001;21:120–7.
[34] Zhou M, Rozvany GIN. DCOC: an optimality criteria method for large systems, part I: theory. Struct Optim 1993;5:12–25.
[35] Sigmund O. On the design of compliant mechanisms using topology optimization. Mech Struct Mach 1997;25:495–526.
[36] Bendsøe MP, Sigmund O. Material interpolation schemes in topology optimization. Achi Appl Mech 1999;69:635–54.
[37] Kim IY, de Weck OL. Adaptive weighted sum method for multiobjective optimization: a new method for Pareto front generation. Struct Multidiscip Optim 2006;31:105–16.
[38] Messac A, Sukam CP, Melachrinoudis E. Mathematical and pragmatic perspectives of physical programming. AIAA J 2001;39:885–93.